MODELING AND SIMULATION OF ELECTROMAGNETIC FIELDS TO MAINTAIN BONE DENSITY DURING PROLONGED LOW GRAVITY EXPOSURE

Austin Tapp[1], Michael Francis[2*], Michel A. Audette[3*]

[1,3] Biomedical Engineering Institute,
[1] Electrical & Computer Engineering;
[3] Computational Modeling & Simulation Engineering
Old Dominion University
5115 Hampton Blvd
Norfolk, VA, USA
atapp001@odu.edu; maudette@odu.edu

[2] Embody LLC
4111 Monarch Way
Suite 510
Norfolk, VA, USA
mpf3b@virginia.edu
*: Advisor

ABSTRACT

Astronauts in long-term, low-gravity environments experience bone density loss at 10 times the rate of those diagnosed with osteoporosis. One treatment effective at maintaining bone density in osteoporotic individuals is electromagnetic field (EMF) therapy. Tools that induce EMFs are becoming increasingly prevalent, but to amplify osteogenesis and encourage superior bone density retention for astronauts, ideal EMF therapy parameters must be determined on patient-specific bases. Therefore, this study explores simulation environments that elucidate highly favorable EMF factors. Pulsed electromagnetic field and combined magnetic field generating devices are variably introduced near patient-specific, finite element (FE) models of the femur, spine, and mandible. The FEs of each model are characterized with tissue conductivity values. Magnetic field strengths obtained along key anatomical regions of the FE models are compared against *in vivo* experimental data to predict features that reflect greater therapeutic impacts. The presented method establishes an adaptable framework for further simulations, which may be modified to test new or existing devices on future patient-specific cases. Using a simulation framework that ratifies parameters for EMF-based bone density retention provides essential insights into combating osteoporosis and negating the similar effects imposed on astronauts enduring prolonged space travel.

Keywords: Modeling & Simulation, Patient-Specific, Electromagnetic Field, Osteoporosis, Bone Density

Introduction

Background

Due to the lack of gravity, astronauts can suffer detrimental bodily impacts over prolonged weightless periods[1,2]. Particularly, two severe complications include kidney stones and bone density loss. To reduce bone density loss, International Space Station crew members exercise a minimum of 15 hours a week, however, this does not fully neutralize the effects of low-gravity[3]. The primary cause of astronauts' bone density loss is minimal osteogenic loading, which results in decrease bone formation and increased bone reabsorption, as osteoblast and osteoclast activity decreases and increases, respectively[4]. Without adequate load, the proximal femoral bone can lose 10% of its mass in 6 months. Recovery time from such a severe degree of bone loss is around 4 years, after returning to Earth[5]. This rate of bone density loss is about 10 times greater than the rate of loss that occurs in individuals diagnosed with osteoporosis. As ISS astronauts endure expeditions that traditionally last six months at a time, a solution to counteract bone density

loss continues to be of significant interest[6]. Additionally, the National Aeronautical and Space Administration is currently focused on deep space exploration and long-term space travel[7]. These expeditions will undoubtably last longer than 6 months and therefore require advanced health support measures to ensure the wellbeing of the astronauts undergoing such missions.

Osteoporosis

This study's application also extends to individuals suffering from osteoporosis. Osteoporosis is a disease that primarily affects older persons, especially women, and occurs when bone growth of osteoblasts is outperformed by bone reabsorption of osteoclasts[8]. When the bone density of an individual is inferior by 2.5 standard deviations compared to the density of a normal adult, that individual is diagnosed with osteoporosis. It is estimated over 200 million people suffer from osteoporosis worldwide and of those diagnosed, 40% have sustained at least one osteoporosis related fracture[9,10]. The cost of these fractures were estimated to be $16 billion in 2002 and $22 billion in 2008[11]. As worldwide demographics continue to shift toward an aged population this problem will reach epidemic level proportions in upcoming decades[8]. An inexpensive, guaranteed, preventative and therapeutic treatment that negates the effects of osteoporosis would be exceptionally beneficial for the geriatric healthcare field.

Electromagnetic Field Therapy

One treatment option for maintaining bone density in both astronauts and those suffering from osteoporosis is electromagnetic field (EMF) therapy. Clinically used EMF generating devices are classified based on their mechanism of action: pulsed electromagnetic field (PEMF) or combined magnetic field (CMF). Both types of EMF therapies have been shown to be safe, effective, and noninvasive methods that promote bone growth *in vitro* and *in vivo*[12 - 17]. Further, EMF treatment significantly improves the intrinsic material properties of bone, including maximum stress, yield stress and toughness, bone mass, bone microstructure, and bone strength[12,18,19]. While PEMFs have bursts, or pulses, of current, CMFs apply continuous current through a combination of alternating and direct current[16,20]. For CMF devices, therapy sessions are about 30 minutes, but for PEMF devices sessions may last a few hours. Regardless of the device used, the cellular impacts of applied EMFs induce the same anabolic upregulation activity. EMFs promote osteogenic differentiation by simultaneously activating the bone morphogenetic proteins, Smad 1/5/8 and BMPRII, to elicit a cascade pathway that induces osteogenesis [14,21]. In clinical use, PEMF treatment is more commonplace for osteotomy and dental implant procedures, during bone regrowth post-fracture and in cases of postoperative osseous consolidation following varus deformity corrections[22-26]. Additionally, many studies have explored PEMF therapy on osteoporotic animal models and in humans diagnosed with osteoporosis[12,18,19,27,28]. Alternatively, CMFs are reportedly more effective at bone regrowth in thoracolumbar spinal regions, after spinal fusion operations and, while not statistically significant, appear to be more successful in bone-tendon junction healing studies. In many clinical trials, results reflect mixed efficacy related to EMF therapy usage for maintaining bone density, however, studies cite challenges in obtaining and determining ideal device position, orientation, and tissue targets throughout osteoporosis treatment[12]. Thus, the present study utilizes an *in silico,* simulation framework that permits device and patient-specific evaluation for ideal EMF therapy factors. The environment seeks to provide risk-free selection and exploration of EMF devices, device position and orientation, and

targeted tissue areas to calculate EMF strength information that guides therapy choices for astronauts and individuals with osteoporosis. Determination of EMF treatment parameters in this manner may boost osteogenesis and support elevated bone density levels to make EMF use a more viable therapy option.

Methods

In Silico Simulation Environment

Some EMF simulation toolkits are provided by software packages such as COMSOL, SolidWorks, Ansys, or Altair Feko. The EMF simulations of these programs are modeled with the Maxwell-Faraday equation for electromagnetism, represented as a differential equation in SI units:

$$\nabla x\, E = -\partial B/\partial t \qquad (1)$$

where E is the electric field and B is the magnetic field. While magnetic field strength is quickly determined with these packages, the studies using such software are required to represent different portions of the bone, cancellous, cortical, and red and yellow marrow, by lumping them into a conglomerate that has shared electrical conductivities[24]. Some studies do provide differing conductivity values for of the inner and outer vertebrae, intervertebral discs, and surrounding mediums, but fail to consider the most critical point of interest of EMF stimulation: the marrow of the bones that contain the mesenchymal stem cells, which give rise to the osteoblasts through the upregulation of the osteogenesis pathway[20]. Further, the studies models in the EMFs simulations are simplistic representations of the true anatomy[24]. Attempting EMF therapeutic standardization with coarse, generalized methodology may be the cause of EMF application challenges reported by clinical trials. In contrast, the present study utilizes patient-specific data and adapts to individualistic anatomy for accurate parameter determination. Additionally, because this study identifies ideal magnetic field positioning, only a single time point needs to be observed, so modeling with electrostatics and magnetostatics is more appropriate than modeling EMFs through eq. 1. Thus, the environment selected for this study was SciRun, from the University of Utah's Scientific Computing and Imaging Institute[29]. SciRun is open-source, highly customizable and permits exploration of static EMFs[30]. In SciRun, imported FE models may be controlled at higher resolutions and are assigned with tissue-specific conductivities along individual tetrahedra for more precise EMF calculations compared to some commercially available toolkits.

Patient-Specific Model Generation:

The femur, spinal vertebra, and mandible are the most common bones to undergo EMF treatment therapy. Developing these models to be patient specific for use in SciRun is accomplished through the same, 6-step pipeline. First an anatomist-drawn, generic, Computer-Aided Design (CAD) template of the anatomy is obtained[31]. The templates are converted into a triangulated surface mesh and characterized with points. Next, corresponding anatomy from a patient image, which may be a computed tomography (CT) or magnetic resonance image (MRI), is segmented. Segmentations are obtained automatically with convolutional neural networks or manually with thresholding and region growing. Then, segmentations are assigned with points homologous to those on the surface mesh. The point pairs allow for an initial affine transformation, which is followed by elastic deformations[32]. The elastic transform mechanism lumps all triangular mesh vertices as mass particles and drives them toward the segmentation, which is specified as the target. During deformation, regularization is applied to penalize inappropriate distortions, internal forces are

incorporated to encourage mesh smoothness and shape similarity, and the local vertex geometries are modeled with mean value encoding. By beginning with a generic mesh and warping it to be patient specific, features of pathological anatomy, such as fractures, are not present, whereas these pathologies would exist in the segmentation. This is critical for the seamless production of an FE model, which is obtained through tetrahedralization of the patient-specific surface mesh. Holes in patient segmentations due to pathology would greatly challenge the tetrahedralization process. The software used to create the volumetric FE models was Cleaver or CGAL, depending on the anatomy to be converted[33,34]. Finally, the FEs of the volumetric models were assigned conductivity values equal to experimentally determined cellular conductivity of the given region[35]. For example, FEs were set to be 9.1 mS/m for cortical bone, 31mS/m for trabecular bone, and 230 mS/m for bone marrow in the femur.

EMF Computation:
The calculation of the EMF strength is dependent on device selection, position, and orientation as well as the chosen anatomy model and its associated conductivity values. In SciRun, EMF emitting devices can be manipulated and even created by a user. Some existing, real-world devices include single cone and double cone coils, a figure 8 coil from Magstim, and the MC-B70 butterfly figure 8 coil from Medtronic. EMFs may be approximated by several magnetic dipoles. The dipoles describe the magnetic field the coil emits and depend on coil shape and other specifications. Typically, these devices are comprised of single or double rings, which have subcoils wound in the opposite direction to focus magnetic stimulation at their midpoints. Electrical current induced by the coils is solved with the following equation:

$$J = -\sigma(\nabla\phi + \frac{dA}{dt}), \qquad (2)$$

where $\nabla\phi$ is the gradient of electrical potential, dA/dt is the time derivative of the magnetic vector potential that is generated by the coil, and $-\sigma$ is the electrical conductivity tensor. As mentioned, the primary current, J, is assumed to be constant for a considered instance in SciRun. Thus, current is dependent on just the position, orientation, and EMF profile of the coils as well as the conductivity of the mesh. Primary current is calculated along every tetrahedra of the entire FE model and a uniform current is at output each element. Therefore, magnetostatic field strength approximation at a position, r, in 3-dimensional space is obtained by the Biot-Savart law of constant uniform current:

$$B(r) = \frac{\mu_0}{4\pi} I \int_C \frac{d\ell \times \hat{r}'}{|r'|^3} \quad (3)$$

where μ_0 is the magnetic constant, I is current, C is the path of the current, and $d\ell$ is a vector along C. The magnetic field values, B, are then compared to experimental studies to evaluate the efficacy of devices' position, orientation, and EMF profile when therapy is being applied to the given point of interest, r.

Results

Patient FE Models
Patient-specific finite element models of the femur, spinal vertebra and mandible were generated via the process outlined above. Using uniform assumptions of cortical bone, trabecular bone, and bone marrow, the FE models were then volumetrically characterized at $0-3mm^3$, $3-24mm^3$ and $24-30mm^3$ for the femur, at $0-2.5mm^3$, $2.5-20mm^3$ and $20-24mm^3$ for the vertebrae and $0-1.5mm^3$, $1.5-6.5mm^3$ and $6.5-8.0mm^3$ for the mandible. The 0mm point occurs on the FE model's surface and final value associated with bone marrow is the model's core; the femur's center is $30mm^3$, the vertebrae centers are $24mm^3$ and the manible's center is $8.0mm^3$. Model generation accuracy was determined prior to the instancing of the models within SciRun. Validation of deformed models meshes was

completed using associated ground truth segmentations. All model fits were evaluated with Dice similarity coefficient (DSC) and average Hausdorff distance using the segmentation comparison tools of 3D Slicer. DSC of femurs had scores of 0.83 and an average Hausdorff distance of 2.37 mm. DSC of vertebral fits had a score of 0.77 and an average Hausdorff distance of 1.4 mm. DSC of manible fits scored 0.81 and had an average Hausdorff distance of 1.18 mm. Figure 1 displays qualitative fitting results and Table 1 summarizes the quantitative results.

Anatomy	DSC (%)	Hausdorff (mm)
Femur	83	2.37
Vertebrae	77	1.4
Mandible	81	1.18
All	80	1.65

Table 1: The DSC and Hausdorff distance metrics of the surface model after patient-specific deformation.
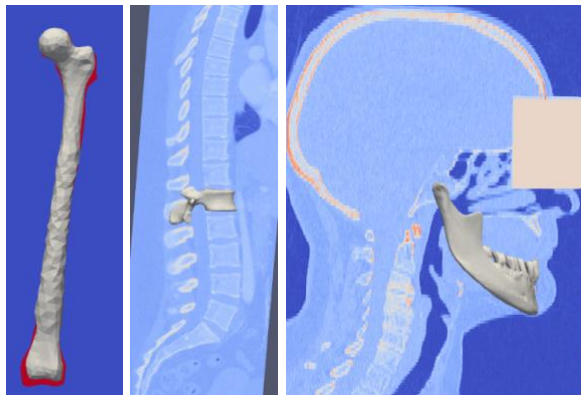

Figure 1: Qualitative views of a femur (left), vertebra (middle) and mandible (right) fitting.

Within the SciRun environment, these patient-specific, FE models assigned particular bone conductivity values. Different views of the volumetric models, which have been clipped to expose the tetrahedra they contain, can be seen in Figure 2 and 3. The clipping plane, appearing in blue, is used to provide cross-section viewing. Figure 4 displays the part of the SciRun interface that is used to assign portions of the FE models with appropriate conductivity values.
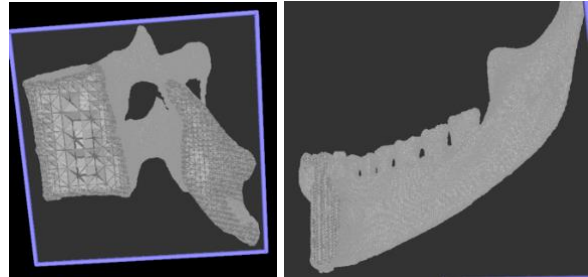

Figure 2: The tetrahedralized vertebra (left) and mandible (right) mesh seen in SciRun.
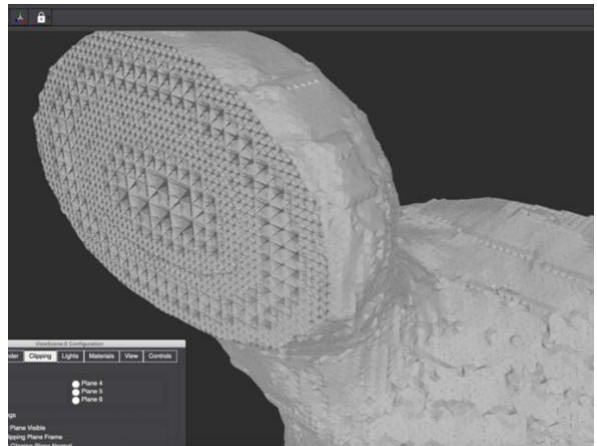

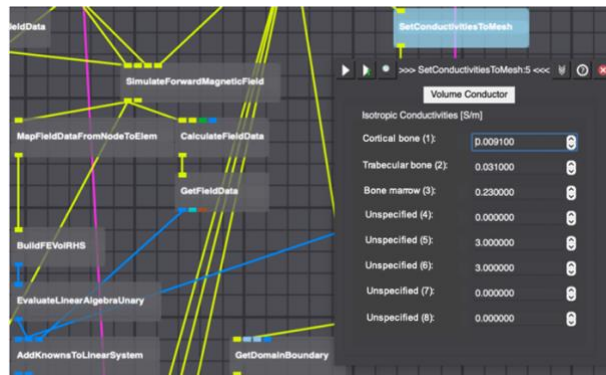Figure 3: A magnified view of femoral head of tetrahedralized femur mesh.

Figure 4: The SciRun interface that also displays the module for setting the mesh conductivity values.
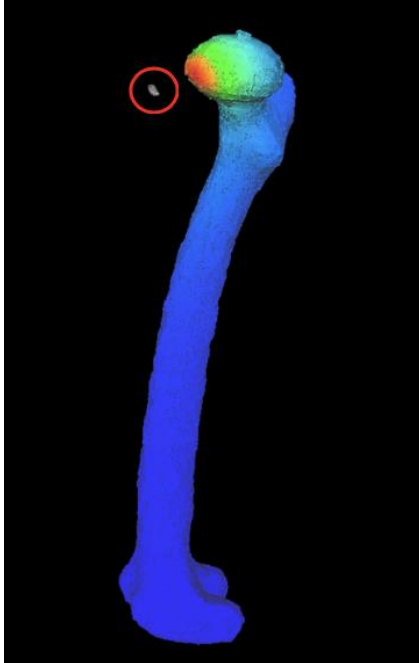
Figure 5: Magnetic field strength intensities on a femur mesh when a EMF device was placed near the femoral head. The device is the small gray blob near the top of the femur, circled in red. Red coloration is maximum field strength intensity while blue coloration is 0 tesla intensity.

Figure 6: EMF strength intensities on the femur mesh when a TMS device was placed near the femoral neck.

Figure 7: EMF strength intensities on the femur mesh when a TMS device was placed near the femoral shaft. In this instance, it is more obvious that the device is emitting two magnetic fields from each of its coils.
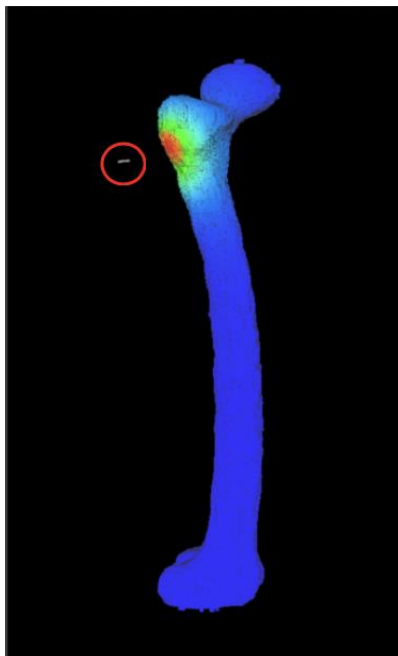
SciRun and Experimental EMF Evaluation
Multiple magnetic field generating devices were placed around the volumetric models to explore how device positional and orientation determines EMF strength. Examples of variable placement on a femur are shown in Figures 5, 6 and 7. The output of the magnetic field intensity on the patient-specific FE models is represented by Tesla units. For each of the mesh types, varied regions of interest were explored. The femur typically loses most bone density around the head, neck, and shaft, so EMF devices were placed near these regions. Because the mandible is subjected to EMF therapy following implantation, probable implant points were targeted. The vertebrae tend to be treated from a posterior position and EMF devices were placed accordingly. Additionally, devices were varied while positioning was maintained; these results can be seen by Figures 8 and 9. The quantitative outputs of the simulations are shown in Tables 2, 3, and 4. When viewing EMF values from

relevant experimental studies magnetic field peak-to-peak observations were generally around 0.0005 T. Some max magnetic field values might reach up to 12 T at target zones.

Values in the following tables that are between or greater than the minimum and maximum field strengths collected during experimental studies are italicized.
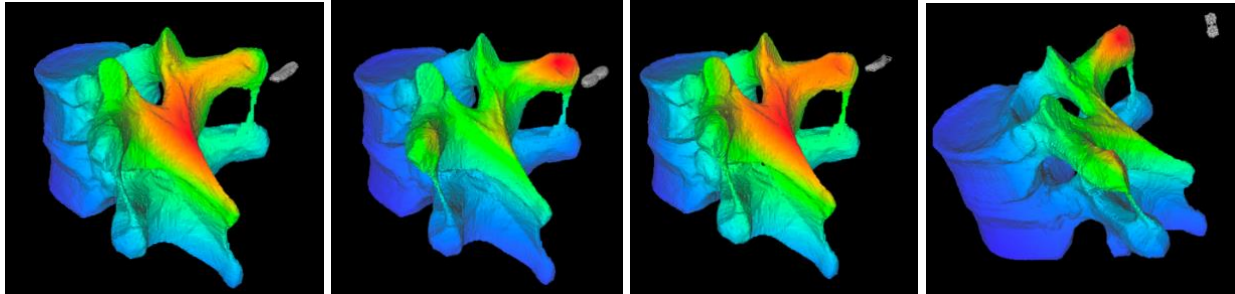

Figure 8: During vertebrae testing, devices are varied while positioning remains consistent. MC-B70 (far left), the Magstim (midleft), single cone (mid right), and double cone X (far right). Red coloration is maximum field strength intensity while blue coloration is 0 tesla intensity.
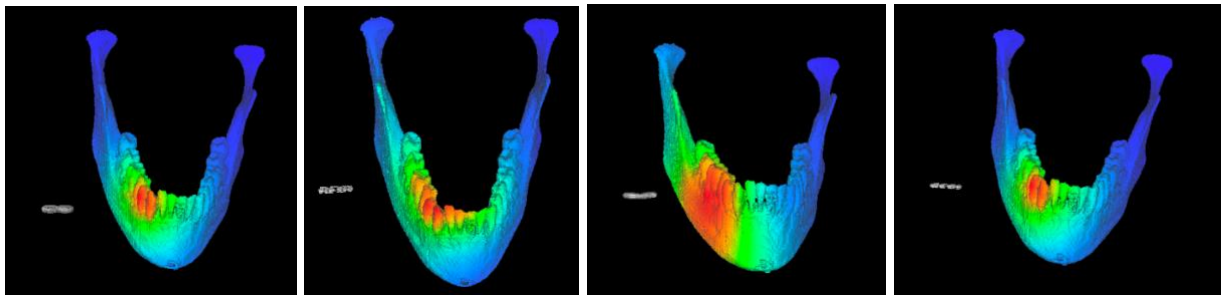

Figure 9: Mandible testing; devices are again varied while positioning remains consistent. The MC-B70 (far left), the Magstim (midleft), single cone (mid right), and double cone X (far right). Red coloration is maximum field strength intensity while blue coloration is 0 tesla intensity.

Device near:	Femoral Head	Femoral Neck	Femoral Shaft
Device	C, T, M (Tesla 10^{-3})	C, T, M (Tesla 10^{-3})	C, T, M (Tesla 10^{-3})
MedtronicMC-B70	*4.1, 4.4, 4.3*	*3.9, 3.5, 3.4*	*1.2*, 0.1, 0.05
Magstim Figure 8	*3.6, 4.2, 4.5*	*3.4, 3.5, 3.9*	*1.1, 0.9*, 0.03
Single Cone Coil	*25, 36, 37*	*26, 27, 28*	*15, 11, 6*
Double Cone Coil	*4.3, 4.9, 4.6*	*4.5, 4.6, 4.7*	*8.7, 7.6, 7.2*

Table 2: The average, magnetic field intensity, in Tesla units for at cortical (C), trabecular (T) and marrow (M) regions while four different EMF devices placed near the femoral head, neck and shaft. Italicized values are between or greater than the ranges of experimentally determined values from appropriately comparable studies.

	TMS Device Placed near: Vertebrae - Magnetic Field Intensity (T, 10^{-3})		
Device	Cortical (Avg., Std., Max)	Trabecular (Avg., Std., Max)	Marrow (Avg., Std., Max)
MedtronicMC-B70	*19, 12, 66*	*20, 13, 64*	*16, 9, 55*
Magstim Figure 8	*17, 13, 55*	*15, 14, 52*	*9, 7, 29*
Single Cone Coil	*68, 64, 336*	*54, 50, 320*	*45, 34, 108*
Double Cone Coil	*20, 14, 69*	*19, 13, 63*	*15, 14, 49*

Table 3: This table reflects the average, standard deviation and maximum magnetic field intensity, in Tesla units, for four different TMS devices placed near vertebrae.

	TMS Device Placed near: Mandible - Magnetic Field Intensity (T, 10^{-3})		
Device	Cortical (Avg., Std., Max)	Trabecular (Avg., Std., Max)	Marrow (Avg., Std., Max)
MedtronicMC-B70	*18, 14, 64*	*18, 15, 61*	*11, 6, 47*
Magstim Figure 8	*15, 12, 44*	*13, 9, 28*	*8, 7, 21*
Single Cone Coil	*66, 60, 332*	*57, 49, 327*	*76, 30, 155*
Double Cone Coil	*19, 15, 62*	*18, 16, 59*	*13, 9, 48*

Table 4: This table reflects the average, standard deviation and maximum magnetic field intensity, in Tesla units, for four different TMS devices placed near the mandible.

Conclusion

A comparison of the experimental data and the EMF values obtained in this study validate the efficacy of the presented simulation methods. The environment proposed by this study provides a foundation for adjustable and seamless integration of new or existing EMF generating devices for patient testing. This testing may be done in a risk-free manner, *in silico,* to determine ideal parameters such as device orientation and position, and even suggest specific benefits of a particular device of choice. Additionally, using the methods outlined above, individualized anatomy may be loaded with conductivity properties to permit greater understanding of EMF effects during therapeutic application on osteoporotic-like bone density degradation. Such data may offer essential insight into necessary protocols for maintaining bone mass in astronauts undergoing expeditions to the International Space Station, Mars, or elsewhere. Furthermore, refining EMF therapies may enhance the lives of millions who are burdened with osteoporosis by reducing their morbidity through increased bone density and substantially decreasing the number of fracture injuries secondary to this disease.

Conflicts of Interest

The authors have no conflicts of interest to declare at this time.

References

1) Abadie, L. J., Lloyd, C. W., & Shelhamer, M. J. (2015). Gravity, Who Needs It? NASA Studies Your Body in Space What.

2) Lev, M. H. (2020). The Long-term Effects of Spaceflight on Human Brain Physiology. *Radiology*, 201164.

3) Dunbar, Brian. "Preventing Bone Loss in Space Flight with Prophylactic Use of Bisphosphonate: Health Promotion of the Elderly by Space Medicine Technologies." *NASA*, 27 May 2015,

4) Selvamurugan, N., Kwok, S., Vasilov, A., Jefcoat, S. C., & Partridge, N. C. (2007). Effects of BMP-2 and pulsed electromagnetic field on rat primary osteoblastic cell proliferation and gene expression. *Journal of Orthopaedic Research*, *25*(9), 1213–1220.

5) Nagaraja, Mamta. "Space Bones." *NASA*, NASA, 1 Oct. 2001

6) Garcia, Mark. "International Space Station Facts and Figures." *NASA*, 28 Apr. 2016.

7) Whiting, Melanie. "NASA Deep Space Exploration Systems Look Ahead to Action-Packed 2018.", 5 Jan. 2018

8) Riggs', B. L., & Melton, L. J. (1995). *The Worldwide Problem of Osteoporosis: Insights Afforded by Epidemiology. Bone*

9) Al Anouti, F., Taha, Z., Shamim, S., Khalaf, K., Al Kaabi, L., & Alsafar, H. (2019). An insight into the paradigms of osteoporosis: From genetics to biomechanics. *Bone Reports*, *11*

10) Halbout, Phillipe. 2017. "Epidemiology." *International Osteoporosis Foundation*.

11) Blume, S. W., & Curtis, J. R. (2011). Medical costs of osteoporosis in the elderly Medicare population. In *Osteoporosis International* (Vol. 22, pp. 1835–1844). Osteoporos Int.

12) Jing, D., Cai, J., Li, F., Xu, Q., … Luo, E. (2014). Pulsed Electromagnetic Fields Partially Preserve Bone Mass, Microarchitecture, and Strength by Promoting Bone Formation in Hindlimb-Suspended Rats. *Journal of Bone and Mineral Research*, *29*(10), 2250–2261.

13) Prakash, D., & Behari, J. (2009). Synergistic role of hydroxyapatite nanoparticles and pulsed electromagnetic field therapy to prevent bone loss in rats following exposure to simulated microgravity. *International Journal of Nanomedicine*, *4*, 133–44.

14) Xie, Y., Shi, W., … Fang, Q., (2016). Pulsed electromagnetic fields stimulate osteogenic differentiation and maturation of osteoblasts by upregulating the expression of BMPRII localized at the base of primary cilium. *Bone*, *93*, 22–32.

15) Ryaby, J. T., Mohan, S., Magee, F. P., & Baylink, D. J. (1995). CMFs increase insulin-like growth factor-ii in te-85 human osteosarcoma bone cell cultures. *Endocrinology*, 136(7), 3100–3106.

16) Cheaney, B., El Hashemi, M., Obayashi, J., & Than, K. D. (2020). CMF results in higher fusion rates than PEMF bone stimulation after thoracolumbar fusion surgery. *Journal of Clinical Neuroscience*, 74, 115–119.

17) Hu, J., Zhang, T., Xu, D., Qu, J., Qin, L., Zhou, J., & Lu, H. (2015). CMF accelerate bone-tendon junction injury healing through osteogenesis. *Scandinavian Journal of Medicine and Science in Sports*, 25(3), 398–405.

18) Topal, O., Çina Aksoy, M., Ciriş, İ. M., Doğuç, D. K., Sert, S., & Çömlekçi, S.

(2020). Assessment of the effect of PEMF application on the healing of bone defects in rats with heparin-induced osteoporosis. *Electromagnetic Biology and Medicine*, 39(3), 206–217.

19) Liu, S., Bi, J., Zhang, Y., Song, Q., Yu, M., Sun, X., … Liu, S. (2020). Preliminary study on the EMF treatment of osteoporosis in rats. *Technology and Health Care*, 28(S1), S47–S55.

20) Stippick, T. W., & Sheller, M. R. (2016). CMFs provide robust coverage for interbody and posterolateral lumbar spinal fusion sites. *Medical & Biological Engineering & Computing*, 54, 113–122.

21) Wang, T., Yang, L., …He, C. (2019). Pulsed electromagnetic fields: promising treatment for osteoporosis. *Osteoporosis International*.

22) Nayak, B. P., Dolkart, O., … Shibli, J. A. (2020). Effect of the PEMF on dental implants stability: A randomized controlled clinical trial. *Materials*, 13(7).

23) Ziegler, P., Nussler, A. K., … Ehnert, S. (2019). PEMF Therapy Improves Osseous Consolidation after High Tibial Osteotomy in Elderly Patients—A Randomized, Placebo-Controlled, Double-Blind Trial. *Journal of Clinical Medicine*, 8(11), 2008.

24) Zborowski, M., Androjna, C., Waldorff, E. I., & Midura, R. J. (2015). Comparison of Therapeutic Magnetic Stimulation with Electric Stimulation of Spinal Column Vertebrae. *IEEE Transactions on Magnetics*, 51(12).

25) Garland DE, Moses B, Salyer W. Long-term follow-up of fracture nonunions treated with PEMFs. *Contemp Orthop*. 1991;22(3):295-302.

26) He, Z., Selvamurugan, N., Warshaw, J., & Partridge, N. C. (2018). Pulsed electromagnetic fields inhibit human osteoclast formation and gene expression via osteoblasts. *Bone*, 106, 194–203.

27) Tabrah, F., Hoffmeier, … Bassett, C. A. L. (1990). Bone density changes in osteoporosis-prone women exposed to pulsed electromagnetic fields. *Journal of Bone and Mineral Research*, 5, 437–442.

28) Huang, L. Q., He, H., He, C., Chen, J., & Yang, L. (2008). Clinical update of pulsed electromagnetic fields on osteoporosis.

29) SCI Institute. (2016). SCIRun: A Scientific Computing Problem Solving Environment. Version 5.0-beta.

30) SCI Institute. (2016). SCIRun Brain Simulator toolkit. Version 1.2.

31) https://cghero.com/

32) Damopoulos, D., Lerch, T. D., …Schmid, J. (2019). Segmentation of the proximal femur in radial MR scans using a random forest classifier and deformable model registration. *International Journal of Computer Assisted Radiology and Surgery*, 14(3), 545–561.

33) CIBC - Scientific Computing and Imaging (SCI) Institute. (2016). Cleaver: A MultiMaterial tetrahedral meshing Library and Application. Version 2.4.

34) https://www.cgal.org/

35) Balmer, T. W., Vesztergom, S., Broekmann, P., Stahel, A., & Büchler, P. (2018). Characterization of the electrical conductivity of bone and its correlation to osseous structure. *Scientific Reports*, 8, 1.

36) López, E., Ibarz, E., Herrera, A., Puértolas, S., Gabarre, S., Más, Y. et al. (2016). A predictive mechanical model for evaluating vertebral fracture probability in lumbar spine under different osteoporotic drug therapies. *Computer Methods and Programs in Biomedicine*, 131, 37–50.